Eur. Phys. J. D **10**, 265–277 (2000)

THE EUROPEAN PHYSICAL JOURNAL D

EDP Sciences

Introduction of quantum finite-size effects in the Mie's theory for a multilayered metal sphere in the dipolar approximation: Application to free and matrix-embedded noble metal clusters

J. Lermé[a]

Laboratoire de Spectrométrie Ionique et Moléculaire, CNRS and Université Lyon I, Bâtiment 205, 43 boulevard du 11 novembre 1918, 69622 Villeurbanne Cedex, France

Received 15 March 1999 and Received in final form 11 October 1999

Abstract. A mixed classical/quantum model for calculating the optical response of free and matrix-embedded multilayered metal spheres in the dipolar approximation is presented. The conduction electrons are quantum-mechanically treated in the framework of the time-dependent local-density-approximation formalism (TDLDA), whereas the surrounding matrix, the ionic metal backgrounds and the non-metallic materials are classically described through homogeneous charge distributions or/and dielectric media. Except for the TDLDA calculations, the present formalism is completely analytical and can be applied to coated spheres with any number of metal or dielectric layers. Contrary to the previous TDLDA-based models involving an inner or/and an outer dielectric medium (one or two interfaces), all the dielectric effects (screening and absorption) are self-consistently calculated. In particular, the interband transitions and the mutual interplay between the conduction and core electrons are self-consistently treated. The deficiencies of the previous models are analyzed, and the results are compared with the classical Mie's theory, over the entire spectral range. The building-up of the classical absorption spectrum, consisting of the surface plasmon resonance and the interband transitions, is clearly observed as the cluster size increases.

PACS. 36.40.-c Atomic and molecular clusters – 71.45.Gm Exchange, correlation, dielectric and magnetic functions, plasmons – 71.10.-w Theories and models of many electron systems

1 Introduction

The optical properties of small metal particles have been the subject of numerous experimental and theoretical works [1]. As compared to the bulk, small particles exhibit specific properties rooted in the collective excitations of the delocalized conduction electrons. The classical Mie's theory for metal spheres (radius R) subjected to an external electromagnetic field (wavelength λ), is undoubtedly the basic achievement for the thorough understanding of these original properties [2].

In cluster physics the radii of the studied particles lie mostly in the size domain corresponding to the so-called dipolar – or quasi-static – approximation, where retardation effects can be neglected ($R/\lambda \ll 1$). For such nanoparticles the light extinction is exhausted by the dipolar absorption, and no size dependence is predicted, except for a mere scaling volume factor. However most experiments reveal large deviations from the Mie's theory. For instance, with regard to the surface plasmon excitation, the measured frequency is red- or blue-shifted relative to the classical value ω_{Mie}, depending on the metal and/or the experimental conditions [1,3,4]. In the case of matrix-embedded noble metal clusters, especially silver, the Mie's theory provides reasonable estimations and seems to succeed better as compared to alkali species. As a matter of fact, recent TDLDA calculations have pointed out that the agreement is fortuitous and results from the partial balancing of competing size trends induced by, respectively, the electronic spillout at the cluster edge and the lowering of the polarizability of the surface ionic cores with respect to the bulk value [5–8]. Since the experiments on the optical response of nanoparticles aim to probe the electronic structure and the dynamics of the confined conduction electrons, an extension of the "macroscopic" Mie's theory taking into account some quantum finite size effects is highly desirable, irrespectively of its success in some specific cases.

Let us remind that the Mie's theory is basically appropriate to particles large enough, in such a way that the quantum surface effects may be neglected. In particular, in the classical description, a step-function for the electronic surface density is assumed, and a Dirac-function for the field-induced oscillating surface density is predicted. For small clusters M_N, a second length scale has to be introduced, namely the Fermi wavelength of the conduction electron gas $\lambda_{\mathrm{F}} \approx 3.3 r_{\mathrm{s}}$ (r_{s} is the Wigner-Seitz radius characterizing the electron density in the bulk). Typically

[a] e-mail: lerme@hplasim2.univ-lyon1.fr

λ_F is on the order of 10 a.u. (≈ 0.5 nm) and the condition $\lambda_F/R \ll 1$ is not fulfilled. The size-dependent oscillations in the electron density, especially the Friedel surface ones, and the extension of the induced electron density on both sides of the "classical" radius $R = r_s N^{1/3}$, have thus to be included in a self-consistent microscopic quantum model.

Well established formalisms, as the Random Phase Approximation [9] or the TDLDA [10,11], primarily applied to simple Drude-like metal clusters [12], are available for calculating these finite-size quantum corrections. For obvious computational constraints *ab initio* methods cannot be carried out, except for very small sizes [13], and phenomenological descriptions of the ionic background and surrounding matrix (embedded clusters) are necessary. The quantum-mechanics treatment is thus restricted to the conduction electron gas. Jellium-like models involving continuous dielectric media have been reported in order to include dielectric screening effects. Various versions, differing in the explicit – or implicit – assumed approximations, can be found in the literature [5,6,8,14–18]. For instance, in reference [14] devoted to simple metal clusters embedded in a matrix, the screening of both the electron-electron and electron-jellium interactions is only taken into account in the ground-state electron density calculation, when it was subsequently pointed out in reference [15] that the main matrix-induced effect comes actually from the direct dynamical screening of the electron-electron interaction.

As a matter of fact the previously quoted TDLDA-based models involving dielectric media [5,6,8,14–18] suffer from severe deficiencies which will be emphasized in this paper. In the previous approaches dealing with dielectric backgrounds, the standard TDLDA formula, suitable for a simple metal particle, have been directly used with appropriate modifications, instead of deriving beforehand, from the classical model counterpart, a well-founded self-consistent TDLDA-based model in presence of dielectric media. We list the three main encountered deficiencies:

(i) the applied external field is substituted for the actual external field experienced by the electron gas, and the induced density is incorrectly calculated;
(ii) the computed observable $\sigma_e(\omega) = (4\pi\omega/c)\Im[\alpha_e(\omega)]$, namely the imaginary component of the dynamical electron gas polarizability, is assumed to be the – normalized – power dissipated by the conduction electrons, and is thus expected to reproduce quantitatively the absorption spectrum below the interband threshold;
(iii) the real interband excitations, which dominate the absorption spectra in the UV domain and strongly quench the surface plasmon peak in most metals (for instance gold and copper), are not included in the model.

Due to the explicit approximation (iii) the TDLDA-spectra cannot be quantitatively compared to the classical Mie's predictions or the experiments, over the whole spectral range. The above deficiencies will be more lengthily analyzed, and exemplified, in the following.

This work aims to include quantum finite-size effects in the Mie's theory for a free or matrix-embedded multilayered metal sphere [1,19], in the dipolar approximation. As stated previously, *only the conduction electron gas is quantum-mechanically handled*. The optical properties of the various media or ionic metal backgrounds (the inner sphere, layers and matrix) are described through phenomenological dielectric functions. The self-consistent determination of a possible size-dependence of the optical constants of these backgrounds is out of the scope of this hybrid quantum/classical model [20]. Nevertheless such a size-dependence could be phenomenologically included by modifying the involved dielectric functions. The spherical symmetry and the dipolar quasi-static approximation are assumed. As compared to the previous quantum approaches based on the same approximations, all the dielectric effects (screening and absorption) are self-consistently calculated, in particular the real intra- and inter-band excitations and the mutual influence of all the induced charge densities. The model requires simple additional analytical developments, based on classical electrodynamics, with respect to the standard TDLDA formalism appropriate to simple Drude-like metal particles in vacuum.

This paper is organized as follows. In Section 2 the general formalism for any number of layers and interfaces is presented, for both the pure classical and the hybrid classical/quantum models. In Section 3 absorption spectra of free and matrix-embedded silver and gold clusters are displayed and compared with, on the one hand the results of the previous models (Sect. 3.1), on the other hand the Mie's predictions (Sect. 3.2). A detailed analysis emphasizing the deficiencies or approximations in previous theoretical approaches is provided in Section 3.1. The summary of this work is given in Section 4.

Atomic units and relative dielectric functions are used throughout this paper. The notations $\Re[\ ]$, $\Im[\ ]$ and $|\ |$ stand for the real component, the imaginary component and the modulus of complex numbers, respectively. For convenience the evident variable- or parameter-dependence of the various expressions are omitted.

2 Theory

2.1 Classical approach

The system consists of several concentric layers (interface radii R_j) of different materials (dielectric functions ε'_j), centred around a spherical core and embedded in a *non absorbing* matrix (see Fig. 1). The core and layers can be any metal, dielectric medium, or even the vacuum (in order to mimic defects or the local porosity at the outermost interface [6,8]). If necessary the progressive transition in the optical properties from one layer to the neighbouring ones may be eventually taken into account by adding thin shells with intermediate optical constants. The only requirement is the homogeneity of the core, the matrix and the various layers.

The system is subjected to a linearly-polarized external electromagnetic field $\mathbf{E}_{ext}(t) = E_0 e^{-i\omega t}\mathbf{e}_z$ (dipolar approximation). The total induced potential and

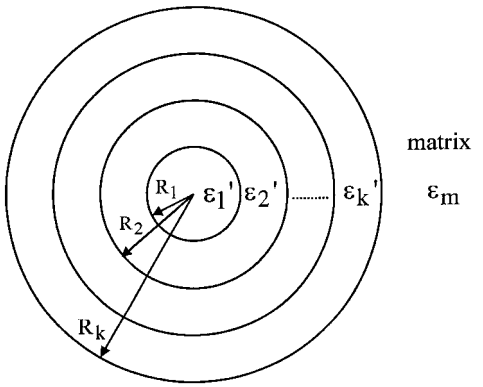

Fig. 1. Model of the matrix-embedded multilayered metal particle. The $\{\varepsilon_i'(\omega)\}$ are the dielectric functions of the various materials.

electric field are of the form $\phi_{\rm c}'(\mathbf{r})\mathrm{e}^{-\mathrm{i}\omega t}$ and $\mathbf{E}(\mathbf{r},t) = -\boldsymbol{\nabla}\phi_{\rm c}'(\mathbf{r})\mathrm{e}^{-\mathrm{i}\omega t}$ [21]. The classical Mie-cross-section corresponding to the dipolar absorption can be obtained by solving the Poisson equation $\Delta\phi_{\rm c}'(\mathbf{r}) = 0$ (no free charge) for the total induced potential $\phi_{\rm c}'(\mathbf{r}) = f_{\rm c}'(r)\cos(\theta)E_0$, with the appropriate boundary conditions at $r = 0$ ($f_{\rm c}'(0)$ is finite), $r = \infty$ ($\mathbf{E}(\mathbf{r},t) = \mathbf{E}_{\rm ext}(t)$) and at the various interfaces (continuity of $f_{\rm c}'$ and of the normal component of the displacement vector, namely $\varepsilon_i'[\mathrm{d}f_{\rm c}'/\mathrm{d}r](R_i^-) = \varepsilon_{i+1}'[\mathrm{d}f_{\rm c}'/\mathrm{d}r](R_i^+)$). The analytical solution of the Poisson equation takes the well-known form

$$\begin{aligned} f_{\rm c}'(r) &= a_1 r \qquad\qquad (r \le R_1) \\ f_{\rm c}'(r) &= -r + \frac{b_m}{r^2} \quad (r \ge R_k) \\ f_{\rm c}'(r) &= a_i r + \frac{b_i}{r^2} \quad (R_{i-1} \le r \le R_i, \quad 1 < i \le k) \end{aligned} \tag{1}$$

where the coefficients a_i and b_i are functions of the interface radii $\{R_i\}$ and dielectric constants $\{\varepsilon_i'(\omega)\}$. Beyond the outermost interface R_k, the total potential is the sum of the applied external potential $-E_0 z\mathrm{e}^{-\mathrm{i}\omega t}$ and the one produced by a time-varying induced dipole $\mathbf{p}_{\rm c}'(t)$ located at the origin in the *homogeneous* matrix

$$\mathbf{p}_{\rm c}'(t) = \varepsilon_m b_m \mathbf{E}_{\rm ext}(t) = \alpha_{\rm c}'(\omega)\mathbf{E}_{\rm ext}(t) \tag{2}$$

$\alpha_{\rm c}'(\omega)$ is the classical *matrix-embedded multilayered particle polarizability*. The power A dissipated by the multilayered particle can be calculated by direct integration over the volume V_i of each absorbing medium (ε_i' complex), according to

$$\begin{aligned} A &= \left\langle \int \Re[\mathbf{E}(\mathbf{r},t)]\frac{\partial}{\partial t}\Re[\mathbf{P}(\mathbf{r},t)]\mathrm{d}\mathbf{r} \right\rangle \\ &= \frac{\omega}{2}\sum_i \Im\left[\frac{\varepsilon_i'-1}{4\pi}\right]\int_{V_i} |\mathbf{E}(\mathbf{r})|^2\,\mathrm{d}\mathbf{r}. \end{aligned} \tag{3}$$

$\mathbf{E}$ and $\mathbf{P}$ are the electric field and polarization vectors, and the symbol $\langle\ \rangle$ stands for the time averaging. A can be alternatively expressed in terms of the induced dipole $\mathbf{p}_{\rm c}'(t)$ subjected to the *applied* external field $\mathbf{E}_{\rm ext}(t)$

$$A = \left\langle \Re[\mathbf{E}_{\rm ext}(t)]\frac{\mathrm{d}}{\mathrm{d}t}\Re[\mathbf{p}_{\rm c}'(t)] \right\rangle = \frac{\omega}{2}\Im\left[\alpha_{\rm c}'(\omega)\right]E_0^2. \tag{4}$$

The classical dipolar absorption cross-section is obtained by dividing the dissipated power A by the incident energy flux inside the matrix $I_0 = cE_0^2[\varepsilon_m]^{1/2}/8\pi$

$$\sigma(\omega) = \frac{A}{I_0} = \frac{4\pi\omega}{c\varepsilon_m^{1/2}}\Im\left[\alpha_{\rm c}'(\omega)\right]. \tag{5}$$

2.2 The mixed classical/quantum model

In the present model the optical response of the conduction electrons in the various metallic materials are microscopically treated within the TDLDA formalism. The electronic gas is then described through an explicit inhomogeneous density $n(\mathbf{r},t) = n_{\rm gs}(\mathbf{r}) + \delta n(\mathbf{r})\mathrm{e}^{-\mathrm{i}\omega t}$, where $n_{\rm gs}(\mathbf{r})$ is the ground state density. In order to be consistent with the usual TDLDA formalism, the electron *charge* density is $-n(\mathbf{r},t)$. Each ionic metal background is phenomenologically described by both:

(i) a homogeneous positive charge distribution $n_i^+(\mathbf{r})$ (jellium approximation), and,
(ii) a homogeneous dielectric medium characterized by the dielectric function $\varepsilon_i(\omega)$, referred to as the "interband contribution" in the following.

Assuming that $\varepsilon_i'(\omega)$ can be split according to $\varepsilon_i'(\omega) = \varepsilon_i(\omega)+\varepsilon_{\rm s}(\omega)-1$, where $\varepsilon_{\rm s}(\omega)$ is the Drude-like contribution related to the conduction electrons, $\varepsilon_i(\omega)$ can be extracted from $\varepsilon_i'(\omega)$ by a Kramers-Kronig analysis [8]. Let us point out that, with respect to the optical excitation, the jellium is inert (*i.e.* no time-varying ionic density $\delta n_i^+(\mathbf{r})$ is induced by the external field), that is all the polarization charges induced in the background are described through the response of the dielectric medium.

As compared to the pure classical model (Sect. 2.1), we are faced – formally – with a "classical" problem almost similar, but involving now dielectric backgrounds with optical constants $\varepsilon_i(\omega)$ ($\varepsilon_i(\omega) = \varepsilon_i'(\omega)$ for non-metallic materials) and free charge densities $\{n_i^+(\mathbf{r})\}$ and $n(\mathbf{r},t)$.

The total *induced* potential $\phi(\mathbf{r}) = f(r)\cos(\theta)E_0$ is now solution of the Poisson equations $\Delta\phi(\mathbf{r}) = 4\pi\delta n(\mathbf{r})/\varepsilon_1$ ($0 \le r < R_1$), $\Delta\phi(\mathbf{r}) = 4\pi\delta n(\mathbf{r})/\varepsilon_i$ ($R_{i-1} < r < R_i$) and $\Delta\phi(\mathbf{r}) = 4\pi\delta n(\mathbf{r})/\varepsilon_m$ ($r > R_k$), with the same boundary conditions as previously except for the replacement of ε_i' by ε_i. The strategy for deriving the present model consists in determining analytically the dipolar coefficient in the long range behaviour of $f(r)$ as a function of the interface radii $\{R_i\}$, the dielectric functions $\{\varepsilon_i\}$ and the induced density $\delta n(\mathbf{r})$, and then calculate self-consistently $\delta n(\mathbf{r})$ by the appropriately-modified basic TDLDA equations.

Due to the linearity of the Poisson equation, $f(r)$ is the sum of two terms ($f = f_{\rm c} + f_{\delta n}$) corresponding, respectively, to the two free charge time-varying sources. The first contribution $f_{\rm c}(r)$ ($\phi_{\rm c}(\mathbf{r}) = f_{\rm c}(r)\cos(\theta)E_0$) corresponds to the charge source implicitly underlain by the

boundary condition at $r = \infty$, that involves the *applied* external field ($\mathbf{E}(\mathbf{r},t) = \mathbf{E}_{\rm ext}(t)$). $\phi_{\rm c}(r)$ is thus solution of the Poisson equation $\Delta\phi_{\rm c}(\mathbf{r}) = 0$. $f_{\rm c}(r)$ is given by the classical solution equation (1), except for the replacement of the parameter-set $\{\varepsilon_i'(\omega)\}$ by the parameter-set $\{\varepsilon_i(\omega)\}$. The corresponding polarizability $\alpha_{\rm c} = \varepsilon_m b_m$ (Eq. (2)) is the one characterizing the induced dipole $\mathbf{p}_{\rm c}(t)$ *in the absence of the electron gas*. Its analytical expression $\alpha_{\rm c}(\{R_i\},\{\varepsilon_i\})$ is the same as the one obtained within the pure classical approach (Sect. 2.1), except for the substitution $\varepsilon_i'(\omega) \to \varepsilon_i(\omega)$. The field $\mathbf{E}_{\rm c}(\mathbf{r},t) = -\boldsymbol{\nabla}\phi_{\rm c}(\mathbf{r})\mathrm{e}^{-\mathrm{i}\omega t}$ will be referred to as the "directly $\mathbf{E}_{\rm ext}(t)$-induced effective external field" for the electron gas. It consists of the applied external field $\mathbf{E}_{\rm ext}(t)$ and the field arising from the polarization charges that are *directly* induced by $\mathbf{E}_{\rm ext}(t)$. Let us point out that the total actual field experienced by the electron gas is the sum of $\mathbf{E}_{\rm c}(\mathbf{r},t)$ and its self-one $\mathbf{E}_{\delta n}(\mathbf{r},t) = -\boldsymbol{\nabla}\phi_{\delta n}(\mathbf{r})\mathrm{e}^{-\mathrm{i}\omega t}$, which includes the contribution arising from the polarization charges that are *directly* induced by $\delta n(\mathbf{r},t)$. This distinction, useful for the following, is introduced for convenience, seeing that – obviously – all the induced dipolar contributions originate, primarily, from the applied field $\mathbf{E}_{\rm ext}(t)$. The second contribution $f_{\delta n}(r)$ is solution of the radial equation

$$\left[\frac{\mathrm{d}^2}{\mathrm{d}r^2} + \frac{2}{r}\frac{\mathrm{d}}{\mathrm{d}r} - \frac{2}{r^2}\right] f_{\delta n}(r) = \frac{4\pi}{\varepsilon_i}\,\delta n(r) \tag{6}$$

where $\delta n(r)$ is defined by $\delta n(\mathbf{r}) = \delta n(r)\cos(\theta)E_0$. $f_{\delta n}(r)$ behaves as $\alpha_{\delta n}/\varepsilon_m r^2$ at long distance, where $\mathbf{p}_{\delta n} = \alpha_{\delta n}(\omega)\mathbf{E}_{\rm ext}(t)$ is the total dipole related to the induced electron density, the relevant induced polarization charges included. $\alpha_{\delta n}$ can be obtained analytically by integrating equation (6) from $r = \infty$ to $r = 0$ and prescribing that $f_{\delta n}(0)$ is finite. The method is outlined in Appendix A

$$\alpha_{\delta n} = \frac{4\pi}{3}\int_0^\infty r^2 f_{\rm c}(r)\delta n(r)\mathrm{d}r. \tag{7}$$

The total dipole of the *matrix-embedded multilayered particle*, *i.e.* the quantum counterpart of equation (2), is therefore

$$\mathbf{p}(t) = \mathbf{p}_{\rm c}(t) + \mathbf{p}_{\delta n}(t) = \alpha(\omega)\mathbf{E}_{\rm ext}(t). \tag{8}$$

$\alpha(\omega) = \alpha_{\rm c}(\omega) + \alpha_{\delta n}(\omega)$ is the *matrix-embedded particle polarizability*. Let us emphasize that the various polarizabilities, in the pure classical model as well as in the present model, are defined relative to the applied external field $\mathbf{E}_{\rm ext}$. The imaginary component of $\alpha(\omega)$ gives the total dipolar absorption cross-section ($\alpha(\omega)$ instead of $\alpha_{\rm c}'(\omega)$ in Eq. (5)). Since the dielectric backgrounds are homogeneous, the dissipated power inside each absorbing medium i can be obtained by the formula equation (3)

$$\begin{aligned} A_i &= \frac{\omega}{2}\Im\left[\frac{\varepsilon_i - 1}{4\pi}\right]\iiint |\mathbf{E}(\mathbf{r})|^2\,\mathrm{d}\mathbf{r} \\ &= \frac{\omega}{2}\Im\left[\frac{\varepsilon_i - 1}{3}\right]E_0^2\int_{R_{i-1}}^{R_i}\left[|\mathrm{d}f(r)/\mathrm{d}r|^2\,r^2 + 2\,|f(r)|^2\right]\mathrm{d}r. \end{aligned} \tag{9}$$

The power dissipated by the conduction electron gas is given by

$$A_{\rm e} = \sigma(\omega)I_0 - \sum_i A_i. \tag{10}$$

Let us emphasize that, when several absorbing media are simultaneously present, the dissipated power by a specific medium has to be evaluated by direct integration through equation (9). The power is not related, as usually assumed in previous works, to the imaginary component of the total dipole corresponding to this medium. Moreover, let us stress that, except for a free particle, both the real and imaginary components of the dipole $\mathbf{p}(t)$ governing the asymptotic behaviour of the potential are different from those of the total dipole of the multilayered particle (integration of the polarization vector over the coated particle volume). As a matter of fact, $\mathbf{p}(t)$ or equivalently the dynamical polarizability $\alpha(\omega)$, is a characteristic of the *matrix-embedded particle*. The reason is that the polarization of the non-absorbing matrix modifies the *effective external field* experienced by the various absorbing media inside the particle (both the in-phase and out-of-phase components, with respect to the phase $\mathrm{e}^{-\mathrm{i}\omega t}$ in $\mathbf{E}_{\rm ext}(t)$, are concerned). These brief remarks will be exemplified in Section 3.1.

The second step in the derivation of the model consists in determining self-consistently the induced electron density $\delta n(\mathbf{r})$. This is achieved by suitably modify the basic ingredients of the TDLDA formalism [10–12], namely the kernel in the integral equation for the density-density correlation nonlocal function $\chi(\mathbf{r},\mathbf{r}')$, and the relationship between the induced density $\delta n(\mathbf{r})$ and the applied external field $\mathbf{E}_{\rm ext}(t)$.

The Kohn-Sham mean field potential in the density functional theory (DFT) (the local approximation is assumed) is

$$V_{\rm eff}(\mathbf{r}, n_{\rm gs}) = \int V_{\rm c}(\mathbf{r},\mathbf{r}')\left[n_{\rm gs}(\mathbf{r}') - \sum_i n_i^+(\mathbf{r}')\right]\mathrm{d}\mathbf{r}' + v_{\rm xc}[n_{\rm gs}(\mathbf{r})]. \tag{11}$$

The first term is the classical Coulomb interaction with all the free and polarization charge densities. $v_{\rm xc}[n_{\rm gs}(\mathbf{r})]$ is the exchange-correlation potential. Let us remind that $n_i^+(\mathbf{r}) = 0$ for non-metallic media. $V_{\rm c}(\mathbf{r},\mathbf{r}')$ is the effective Coulomb interaction between two free elementary charges located at $\mathbf{r}$ and $\mathbf{r}'$ in the presence of the concentric dielectric media $i = 1, 2, \ldots, k, m$, and depends

on the parameter sets $\{R_i\}$ and $\{\varepsilon_i(\omega)\}$. The analytical formula for the simplest cases (one interface ($k = 1$) and two interfaces ($k = 2$)), which depend on the locations of r and r' relative to the interface radius R_1 (radii R_1 and R_2), can be found in references [8,15]. Actually only the $\ell = 0$ (ground-state) and $\ell = 1$ (dynamical screening) components in the multipolar expansion of V_c are involved in the model. For the ground-state calculation the static dielectric constants $\varepsilon_i(\omega = 0)$ are involved in V_c. A formulation involving explicitly the polarization charges in the various media (labelled $n_i(\mathbf{r})$ $(i = 1, 2, \ldots, k, m)$ for both the volume and surface charge densities) is more transparent for the subsequent explanations

$$V_{\text{eff}}(\mathbf{r}, n_{\text{gs}}) = \int \frac{n_{\text{gs}}(\mathbf{r}') - \sum_i [n_i^+(\mathbf{r}') + n_i(\mathbf{r}')]}{|\mathbf{r} - \mathbf{r}'|}\, \mathrm{d}\mathbf{r}' + v_{\text{xc}}[n_{\text{gs}}(\mathbf{r})]. \quad (12)$$

In presence of the applied external field $\mathbf{E}_{\text{ext}}(t)$ the charge distributions acquire an induced oscillating component (except $n_i^+(\mathbf{r})$, since the dielectric properties of the ionic backgrounds are completely described through $\varepsilon_i(\omega)$), *i.e.* $-\delta n(\mathbf{r})\mathrm{e}^{-\mathrm{i}\omega t}$ and $\delta n_i(\mathbf{r})\mathrm{e}^{-\mathrm{i}\omega t} = [\delta n_{\text{ic}}(\mathbf{r}) + \delta n_{\text{ie}}(\mathbf{r})]\mathrm{e}^{-\mathrm{i}\omega t}$. In the last expression the induced polarization charges in the dielectric media have been split into the respective contributions that are directly-induced by the two oscillating free-charge sources, namely the applied field $\mathbf{E}_{\text{ext}}(t)$ (δn_{ic}) and the induced electronic charge $-\delta n(\mathbf{r})\mathrm{e}^{-\mathrm{i}\omega t}$ (δn_{ie}). According to the TDLDA formalism the induced electron density is obtained from the independent-electron density-density correlation nonlocal function $\chi_0(\mathbf{r}, \mathbf{r}')$ provided that the induced time-varying component of the mean field potential $\delta V_{\text{eff}}(\mathbf{r})\mathrm{e}^{-\mathrm{i}\omega t}$ is added to the applied external interaction potential $V_{\text{ext}}(\mathbf{r}, t) = r\cos(\theta)E_0\mathrm{e}^{-\mathrm{i}\omega t}$

$$\delta V_{\text{eff}}(\mathbf{r}) = \int \frac{\delta n(\mathbf{r}') - \sum_i \delta n_{\text{ie}}(\mathbf{r}')}{|\mathbf{r} - \mathbf{r}'|}\, \mathrm{d}\mathbf{r}' + \frac{\partial v_{\text{xc}}[n_{\text{gs}}]}{\partial n}\, \delta n(\mathbf{r}) + \left[V_{\text{ext}}(\mathbf{r}) - \int \frac{\sum_i \delta n_{\text{ic}}(\mathbf{r}')}{|\mathbf{r} - \mathbf{r}'|}\, \mathrm{d}\mathbf{r}' \right]. \quad (13)$$

The first term is the Coulomb interaction with the induced electron density and the directly δn-induced polarization charges. Its expression is nothing else but $\int V_c(\mathbf{r}, \mathbf{r}')\delta n(\mathbf{r}')\mathrm{d}\mathbf{r}'$, where now the dielectric constants $\varepsilon_i(\omega)$ corresponding to the frequency ω have to be used in V_c. The third term $V'_{\text{ext}}(\mathbf{r})$ (square brackets), which does not depend on $\delta n(\mathbf{r})$, is the *effective external interaction potential* for the electron gas and its directly-induced polarization charges, namely the applied external interaction potential $V_{\text{ext}}(\mathbf{r})$ plus the interaction with the directly $\mathbf{E}_{\text{ext}}$-induced polarization charges δn_{ic}. It is thus obvious that $V'_{\text{ext}}(\mathbf{r}) = -\phi_c(\mathbf{r}) = -f_c(r)\cos(\theta)E_0$. The induced electron density $\delta n(\mathbf{r})$ and the correlation function $\chi(\mathbf{r}, \mathbf{r}')$ are therefore obtained from the following modified basic TDLDA-equations

$$\delta n(\mathbf{r}) = \int \chi(\mathbf{r}, \mathbf{r}') V'_{\text{ext}}(\mathbf{r}')\mathrm{d}\mathbf{r}' \quad (14)$$

$$\chi(\mathbf{r}, \mathbf{r}') = \chi_0(\mathbf{r}, \mathbf{r}') + \iint \chi_0(\mathbf{r}, \mathbf{r}_1)K(\mathbf{r}_1, \mathbf{r}_2)\chi(\mathbf{r}_2, \mathbf{r}')\mathrm{d}\mathbf{r}_1\mathrm{d}\mathbf{r}_2 \quad (15)$$

where the kernel $K(\mathbf{r}_1, \mathbf{r}_2)$, the so-called residual interaction, is expressed as

$$K(\mathbf{r}_1, \mathbf{r}_2) = V_c(\mathbf{r}_1, \mathbf{r}_2) + \frac{\partial v_{\text{xc}}[n_{\text{gs}}]}{\partial n}\, \delta(\mathbf{r}_1 - \mathbf{r}_2). \quad (16)$$

The correct integral equation for $\chi(\mathbf{r}, \mathbf{r}')$ has been already involved in some recent works devoted to free and embedded metal clusters [5,6,8]. However the induced density $\delta n(\mathbf{r})$ has been incorrectly calculated by using V_{ext} instead of V'_{ext} in equation (14). In some other works the correct effective external interaction potential V'_{ext} has been involved, but in the framework of "incomplete" or approximate models [16,18]. Especially, in all previous TDLDA-investigations involving dielectric media, the formula $\sigma_e(\omega) = (4\pi\omega/c)\Im[\alpha_e(\omega)]$ has been used for calculating the absorption cross-section, where $\alpha_e(\omega)$ is the dynamical electron gas polarizability

$$\alpha_e(\omega) = -\frac{4\pi}{3} \int_0^\infty r^3 \delta n(r)\mathrm{d}r. \quad (17)$$

The present model clearly stresses that the electronic dipole $\mathbf{p}_e(t) = \alpha_e(\omega)\mathbf{E}_{\text{ext}}(t)$, more precisely $\Im[\alpha_e(\omega)]$, is not the relevant observable, except for simple metal (Drude-like) clusters in vacuum. Moreover, $\sigma_e(\omega)$ is not related to the power dissipated by the electronic gas. This statement holds for both the pure classical and the present models, and will be exemplified in the next section.

It is instructive to relate the dynamical polarizability $\alpha_{\delta n}$ with the density-density correlation function. From equations (7, 15) one can show that

$$\alpha_{\delta n} E_0 = -\int \chi(\mathbf{r}, \mathbf{r}') V'_{\text{ext}}(\mathbf{r}') V'_{\text{ext}}(\mathbf{r})\mathrm{d}\mathbf{r}\mathrm{d}\mathbf{r}'. \quad (18)$$

Equation (18) is nothing else but the generalization of the standard TDLDA formula with V'_{ext} (*effective* external interaction potential) instead of $V_{\text{ext}} = zE_0$ (*applied* external interaction potential). Let us emphasize again that the dynamical polarizability $\alpha_{\delta n}$ includes contributions from *both* the conduction electron gas and the directly δn-induced polarization charges n_{ie}.

3 Application to noble metal clusters

In this section we exemplify the above formalism in the simple cases involving, either a single, or two concentric interfaces. For the purpose of physical interest, the optical response of silver and gold clusters, either free or

matrix-embedded, are calculated. The real and imaginary components of the interband contribution $\varepsilon_1(\omega)$ for these two metals have been extracted from the experimental data by a Kramers-Kronig analysis, and are displayed in references [6,8]. We remind that the interband thresholds (excitations of the d electrons) are about 3.9 eV and 1.9 eV for silver and gold, respectively.

This section is divided into two parts. In Section 3.1 we compare the predictions of the present model with the results obtained within the former theoretical approaches [5–8,14–18]. Previous theoretical studies [6,8] on the size evolution of the surface plasmon band are briefly commented. In Section 3.2 the results of the present hybrid model are quantitatively compared with the predictions of the classical Mie theory. As compared to the former TDLDA-based formalisms, the improvements are unquestionable, over the whole spectral range.

3.1 Comparison with the previous theoretical approaches

The comparison with the former TDLDA-based works is exemplified in the simple case consisting of a metal sphere (radius R_1) in vacuum or embedded in alumina. This matrix is non absorbing in the energy range 0.15–6 eV, and its real dielectric constant $\varepsilon_m(\omega)$ is on the order of 3. The ingredients of the present model in the case of a single interface are given in Appendix B. We remind that in the TDLDA formalism [10–12] the evaluation of the Green's functions $G(\mathbf{r},\mathbf{r}',E) = \langle \mathbf{r} \left| [H - E - \mathrm{i}\delta]^{-1} \right| \mathbf{r}' \rangle$ for calculating the independent-electron nonlocal correlation function $\chi_0(\mathbf{r},\mathbf{r}')$ requires the use of a finite value for the infinitesimal δ-parameter. This amounts roughly to attributing an intrinsic width 2δ to each bound-bound particle-hole excitation line (Lorentzian-shaped peaks). In the present calculations δ is fixed to 100 meV. In most displayed spectra, this value is large enough to smooth out the possible fragmentation pattern due to the coupling of the collective surface plasmon mode with the single particle excitations (Landau damping [22]).

In Figures 2 and 3 are displayed absorption spectra for free and matrix-embedded Au_N and Ag_N clusters. The predictions of the model (Eq. (5) with $\alpha(\omega) = \alpha_c(\omega) + \alpha_{\delta n}(\omega)$ instead of $\alpha'_c(\omega)$, thick line curves) are compared with those obtained when only the electron gas polarizability $\alpha_e(\omega)$ (Eq. (17)) is involved in the general absorption cross-section formula (Eq. (5)). In the two previous approaches the kernel (Eq. (16)) is appropriately modified, and the density-density correlation function $\chi(\mathbf{r},\mathbf{r}')$ (Eq. (15)) is thus correctly calculated. The two models differ in the evaluation of $\delta n(\mathbf{r})$ from equation (14). In the first crude theoretical approach $V_{\mathrm{ext}}(\mathbf{r})$ (the *applied* external interaction potential) is used instead of $V'_{\mathrm{ext}}(\mathbf{r})$ (dashed line curves; model referred to as "model 1"). In the second model $\delta n(\mathbf{r})$ is correctly calculated (thin line curves; model referred to as "model 2"). The present model is referred to as "model 3".

The discrepancies between the various curves are very large, not only in the UV spectral range where the interband excitations – neglected in the previous works – dominate the absorption, but also in the spectral range of the surface plasmon mode. The differences are much more pronounced in the case of free gold clusters, due to the partial quenching of the plasmon band by the interband transitions. The plasmon peak still remains visible, because it is located just above the interband threshold (in gold the imaginary component $\Im[\varepsilon_1(\omega)]$ presents a flat maximum between 3 eV and 5 eV).

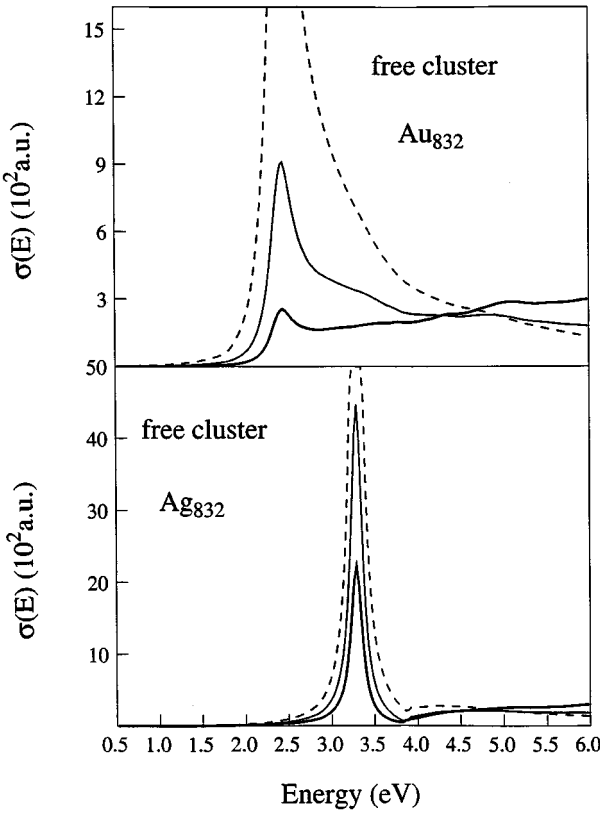

Fig. 2. Photoabsorption spectra of free gold and silver clusters. Thick line curve: result of the present model (model 3). Thin and dashed line curves: results of the previous models (models 2 and 1, respectively). The maxima of the dashed line peaks are about 33 (Au_{832}) and 90 (Ag_{832}).

Despite the deficiencies in the previous approaches one can notice that the peak location, as well as the underlying fragmented pattern (see Fig. 3), are correctly reproduced, especially for silver. This fortunate agreement can be explained by inspecting the explicit formula reported in Appendix B. In the models 2 and 3 $V'_{\mathrm{ext}}(\mathbf{r})$ has different analytical expressions on both sides of the interface, whereas $V_{\mathrm{ext}}(\mathbf{r}) = r\cos(\theta)E_0$ in model 1. If the radial region $r > R_1$ is disregarded, the *approximate* relation $V'_{\mathrm{ext}}(\mathbf{r}) \approx -a_1(\omega)V_{\mathrm{ext}}(\mathbf{r})$ holds. Therefore the induced electronic density and dipole $\mathbf{p}_e = \alpha_e(\omega)E_0\mathbf{e}_z$ are the same in the three models, except for the missing of the scaling factor $-a_1(\omega)$ in the model 1. Consequently, below the interband threshold ($-a_1(\omega)$ is real and positive), the absorption spectra calculated in the two models 1 and 2 differ from each other through a ω-*dependent*

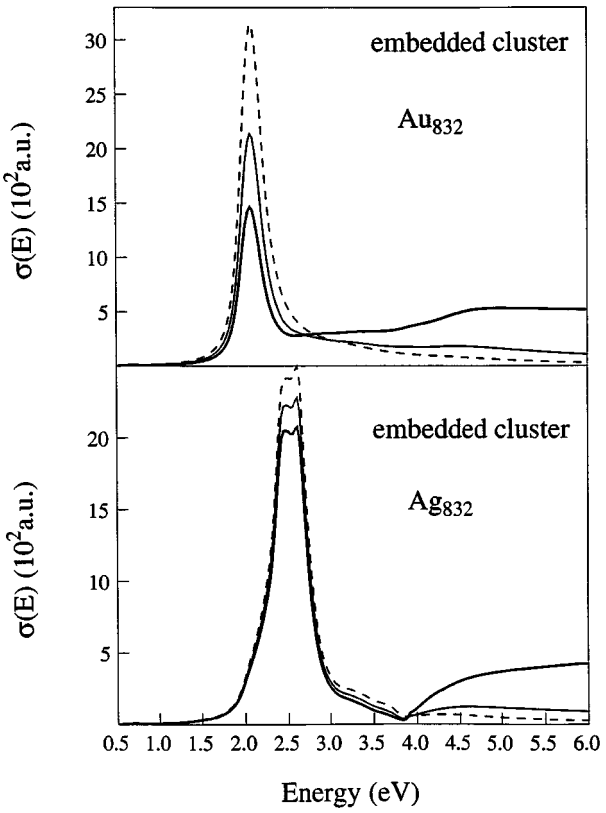

Fig. 3. Same as the caption of Figure 2 for alumina-embedded clusters.

scaling factor. If the plasmon peak-width is small enough, as compared to the spectral range where $a_1(\omega)$ changes noticeably, both the location and the width of the plasmon band are similar in both models 1 and 2, and only the amplitude is different. On the other hand, above the interband threshold, $\chi(\mathbf{r},\mathbf{r}')$, $\delta n(\mathbf{r})$ *and* $V'_{\text{ext}}(\mathbf{r})$ are complex, and the respective imaginary components of $\alpha_{\text{e}}(\omega)$ in the two models 1 and 2 are no longer related by the simple scaling factor $-a_1(\omega)$. This is clearly illustrated in Figures 2 and 3 in the UV spectral range.

Let us now consider the present model and – as done previously – let us disregard the second term in equation (B.3). Below the interband threshold, we have the approximate relations

$$\alpha_{\delta n}(\omega) \approx -a_1\alpha_{\text{e}}(\text{model 2}) \approx a_1^2\alpha_{\text{e}}(\text{model 1})$$

with $-a_1(\omega) = 3\varepsilon_m/(\varepsilon_1 + 2\varepsilon_m)$. We remind that $\alpha_{\delta n}(\omega)E_0\mathbf{e}_z$ includes, in addition to the electronic dipole $\mathbf{p}_{\text{e}} = \alpha_{\text{e}}(\omega)E_0\mathbf{e}_z$, a contribution arising from the dielectric media (polarization charges $n_{1\text{e}}$ and $n_{m\text{e}}$). The above relations point out clearly the deficiencies of the models 1 and 2. In the model 2 $\mathbf{p}_{\text{e}}$ is correctly calculated, but its imaginary component is incorrectly substituted for the one of the total dipole $\mathbf{p}(\omega) = \alpha(\omega)E_0\mathbf{e}_z$ governing the long range behaviour of the potential. Even if the inner dielectric medium is non absorbing in the relevant spectral range, this substitution is unsuitable and leads to erroneous quantitative predictions. The reason is that both the real and imaginary components of the total polarizability $\alpha(\omega) = \alpha_{\delta n}(\omega) + \alpha_{\text{c}}(\omega)$ are *global* properties of the *matrix-embedded metal particle*. Actually $\alpha(\omega)$ is an intrinsic property of the particle (metal sphere) only if $\varepsilon_m = 1$ (vacuum). Moreover, even in the simple case of a *free* metal cluster involving a *non absorbing* inner medium ($\varepsilon_1(\omega)$ is real in the relevant spectral range), the absorption cross-section is not directly given by $\Im[\alpha_{\text{e}}(\omega)]$. In vacuum the total dipole $\mathbf{p}(\omega)$ is obviously the sum of the total dipoles corresponding to, respectively, the conduction electron gas and the inner medium, namely $\mathbf{p} = \mathbf{p}_{\text{e}} + \mathbf{p}_1 = [\alpha_{\text{e}}(\omega) + \alpha_1(\omega)]\mathbf{E}_{\text{ext}}$. However, due to the absorption by the electron gas, the actual field experienced by the inner medium has a component in quadrature with respect to the applied external field $\mathbf{E}_{\text{ext}}(t) = E_0\text{e}^{-\text{i}\omega t}\mathbf{e}_z$. Therefore both $\mathbf{p}_{\text{e}}$ *and* $\mathbf{p}_1$ are complex and contribute to the absorption cross-section formula, although no energy is dissipated in the inner medium 1 ($\Im[\alpha(\omega)] = \Im[\alpha_{\text{e}}(\omega)] + \Im[\alpha_1(\omega)] \approx -a_1(\omega)\Im[\alpha_{\text{e}}(\omega)]$). Actually, when the system consists of several materials, the dissipated power in a specific medium is not related merely to the imaginary component of the corresponding dipole: in the TDLDA-formalism the in-phase and $\pi/2$-out-of-phase components are defined relative to the phase of the applied external field $E_0\text{e}^{-\text{i}\omega t}\mathbf{e}_z$, and not relative to the one of the effective external field experienced locally by the medium. Thus, in most cases, the dissipated power in each homogeneous material has to be calculated by direct integration according to equation (3).

The above comments emphasize the two main points that have been implicitly circumvented, or insufficiently analyzed, in the previous works involving embedded clusters or free clusters consisting of several materials:

(i) the global nature of the overall matrix-embedded metal particle polarizability, and,
(ii) the effective external field (amplitude and phase) experienced locally by each – absorbing or non absorbing – medium and their mutual interplay. All these remarks apply to both the classical and hybrid models.

These remarks can be easily supported – analytically – within the classical Mie theory.

In Figure 4 are shown the various contributions to the overall absorption cross-section $\sigma(\omega)$ (thick line curves). The contribution of $\alpha_{\delta n}(\omega)$ ($\sigma_{\delta n}(\omega) = (4\pi\omega/c\varepsilon_m^{1/2})\Im[\alpha_{\delta n}(\omega)]$; thin line curves), the absorption cross-sections corresponding to the core electrons (*i.e.* A_1/I_0, Eq. (9); dashed line curves) and to the conduction electrons ($\sigma_{\text{e}}(\omega) = \sigma(\omega) - A_1/I_0$; dotted line curve in the upper figure) are displayed. As expected, in silver clusters the conduction electrons are entirely responsible for the surface plasmon band and contribute only very weakly to the absorption in the UV spectral range (this holds true for embedded clusters). On the other hand, for gold clusters, both the conduction and core electrons contribute to the absorption in the visible spectral range, in particular to the collective Mie excitation. This joint contribution is especially striking in the case of free gold clusters,

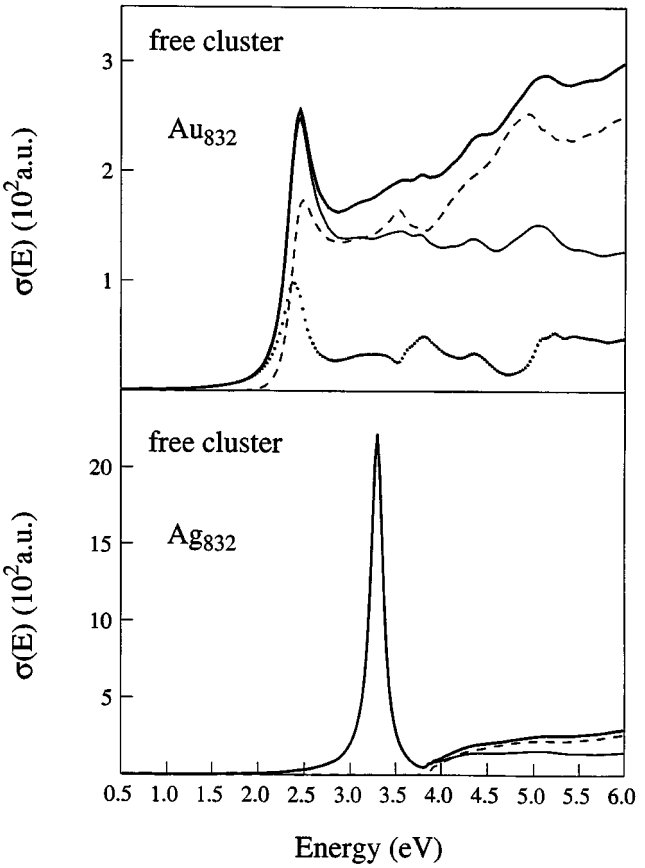

Fig. 4. The various contributions to the overall absorption cross-section $\sigma(\omega)$ (thick line curves). Thin line curves: contribution of the polarizability $\alpha_{\delta n}(\omega)$ (see Eq. (7)). Dashed line curves: contribution of the core electron excitations. Dotted line curve (upper figure): contribution of the conduction electron excitations.

and to a lesser extent for embedded clusters. Actually, when the intra- and inter-band excitations are strongly coupled, the oscillator strength related to the conduction electron excitations is spread over the entire VIS-UV spectral range.

The respective contributions of $\alpha_{\delta n}(\omega)$ and $\alpha_{\rm c}(\omega)$ to the overall absorption cross section deserves a brief comment. Beforehand let us remind that $\Im[\alpha_{\rm c}(\omega)] = 0$ below the interband threshold ($\alpha_{\rm c}(\omega)$ is related to the polarization properties of the inner medium 1 only). Above the interband threshold, both contributions are of the same order of magnitude in the case of silver clusters. In the case of gold, this holds true only far above the threshold. In Figure 4 the contribution of $\alpha_{\rm c}(\omega)$ practically vanishes below 2.8 eV, although the core electrons still contribute largely to the absorption cross-section. The reason is that only the polarizability $\alpha_{\delta n}(\omega)$ reflects the strong enhancement of the effective local field inside the cluster when the collective dipolar mode is excited (the full dielectric function of the metal is implicitly involved in this term).

Owing to the deficiencies of the former models, the size evolution of the surface plasmon frequency in small noble metal clusters have been re-investigated in the framework of this improved formalism. The qualitative and quantitative analyses about the finite-size effects, that were previously reported [6,8], remain suitable. In the case of gold, only a very tiny additional blue-shift of the peak maximum, due to the superimposition with the interband transitions, is observed. Especially, the relevance of both:

(i) the inner surface skin of ineffective screening (thickness d), introduced early by Liebsch in the context of metal surfaces [23], and,
(ii) the interface vacuum rind (thickness d_m) for simulating the local matrix porosity at the particle/matrix interface (embedded clusters), is confirmed.

Experimental results on alumina-embedded Au_N and Ag_N clusters can be found in reference [20] (second reference) and reference [6], respectively. Some theoretical absorption spectra are presented in Section 3.2.

3.2 Comparison with the classical Mie theory

As compared to the classical theory, the present model differs only in the description of the ground-state electron density and its dynamical response to an external electromagnetic field. Therefore the classical polarizability $\alpha'_{\rm c}(\omega)$ (Eq. (2)) has necessary to be recovered if the classical induced electron density $\delta n_{\rm c}(r)$ is used in equation (7). This can be easily checked in the simple case involving a single interface, with $R_1 = R_N$. In the classical model the electric field inside the metal sphere is homogeneous ($\mathbf{E}_{\rm int}(t) = [3\varepsilon_m/(\varepsilon'_1 + 2\varepsilon_m)]E_0 {\rm e}^{-{\rm i}\omega t}\mathbf{e}_z$) and the polarization vector corresponding to the free charge densities (conduction electrons and jellium) is $\mathbf{P}_{\rm int}(t) = [(\varepsilon_{\rm s} - 1)/4\pi]\mathbf{E}_{\rm int}(t)$. The induced polarization charge density related to the Drude contribution in the metal dielectric function ($\varepsilon'_1(\omega) = \varepsilon_{\rm s}(\omega) + \varepsilon_1(\omega) - 1$) is located at the interface, and is equal to

$$\sigma_{\rm c}(\mathbf{r}, t) = \delta(r - R_1)\mathbf{P}_{\rm int}(t)(\mathbf{r}/r) = -\delta n_{\rm c}(r)\cos(\theta)E_0{\rm e}^{-{\rm i}\omega t}$$

with

$$\delta n_{\rm c}(r) = -[(\varepsilon_{\rm s} - 1)/4\pi][3\varepsilon_m/(\varepsilon'_1 + 2\varepsilon_m)]\delta(r - R_1).$$

By using the alternative expression (B.4) in the Appendix B for calculating $\alpha_{\delta n}(\omega)$, it is straightforward to show that $\alpha_{\delta n}(\omega) + \alpha_{\rm c}(\omega) = \alpha'_{\rm c}(\omega)$.

In the following we investigate, on the one hand how far are the classical results in the small-size domain relative to those calculated within the present microscopic TDLDA approach, and, on the other hand, the rate with which the results of the present model converge towards the classical theory as the cluster size increases. This comparative study is carried out in the framework of simple models, involving either one or two interfaces, and exemplified in the case of gold clusters. In order to be consistent with the line-width parameter $2\delta = 0.2$ eV used in the TDLDA calculations (see the beginning of Sect. 3.1), the value $\Gamma = 0.2$ eV is assumed in the Drude dielectric

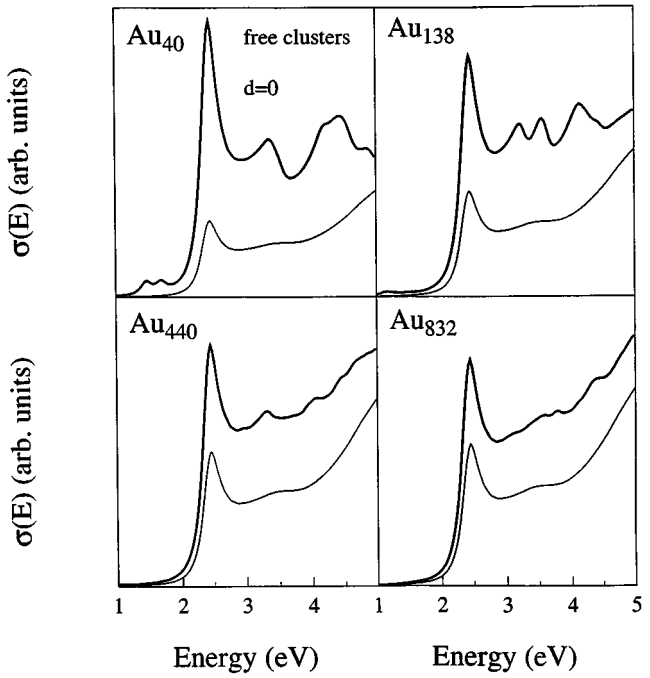

Fig. 5. Comparison between the results of the quantum model (thick line curves) and the classical Mie-theory (thin line curves), for free gold clusters.

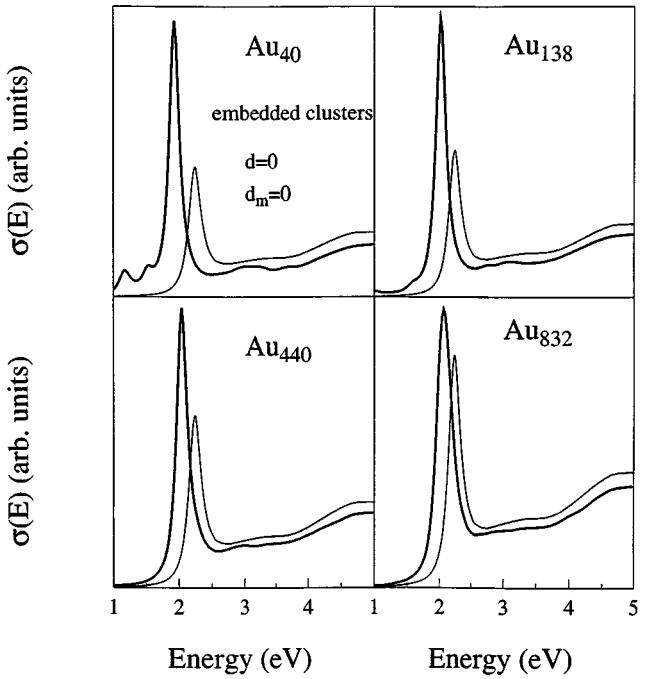

Fig. 6. Comparison between the results of the quantum model (thick line curves) and the classical Mie-theory (thin line curves), for alumina matrix-embedded gold clusters.

function $\varepsilon_{\rm s}(\omega) = 1 - \omega_{\rm p}^2/[\omega(\omega + {\rm i}\Gamma)]$, where $\omega_{\rm p} = (3/r_{\rm s}^3)^{1/2}$ is the bulk plasma frequency. Let us emphasize that this prescription does not imply necessarily that the width of the surface plasmon peak will be identical in both models, since the present TDLDA approach gives rise to finite size effects, in particular the size-dependent Landau fragmentation of the collective mode. In each figure, both spectra have been scaled by the same factor, and can be thus quantitatively compared.

In Figures 5 and 6 are displayed absorption cross-sections for free and alumina matrix-embedded gold clusters, within the standard Mie-like model ($d = d_m = 0$, see the end of Sect. 3.1). We remind that the only size dependence in the classical model is a mere volume scaling factor. Contrary to the previous theoretical models, we see that the magnitude of the absorption cross-sections in the pure classical and hybrid models are now of the same order of magnitude. For free clusters the TDLDA cross-sections are systematically larger, over the entire spectral range. By contrast, the trend is inverted in the case of embedded gold clusters, except in the vicinity of the surface plasmon frequency. In fact this feature is element-dependent. For silver, owing to the gap between the respective spectral ranges involving the conduction and core electron excitations, a quite good quantitative agreement over the whole UV spectral region is observed for any size and for both free and embedded clusters.

With regard to the location of the Mie band, no size effect is observed in the case of free gold clusters, as already pointed out in our early work [8]. At first sight the agreement with the classical predictions is surprising, since the quantum spillout phenomenon is not taken into account within the Mie theory. Actually this agreement is fortuitous and results from the exact balancing between:

(i) the spillout-induced red-shift trend, and,
(ii) the simultaneous blue-shift trend due to the fact that the Coulomb interaction is less screened for the electrons lying beyond the cluster surface.

For silver clusters the surface plasmon frequency calculated within the quantum model is red-shifted with respect to the classical value, suggesting that the balancing is not perfect in this case. In silver the screening by the ionic background polarization is lower, as compared to gold (in the spectral range of their respective Mie-frequency $\Re[\varepsilon_1(\omega)] \approx 4.5$ and ≈ 10, for silver and gold, respectively). Therefore, in silver clusters, the spillout-induced red-shift trend has a stronger relative influence on the overall size effects.

In the case of embedded clusters, both the electron spillout and the Coulomb-interaction screening beyond the surface are enlarged, as compared to free clusters. The TDLDA Mie-band is thus red-shifted relative to the classical one, and exhibits moreover a red-shift trend as the cluster size decreases. In the case of gold, this red-shift towards the threshold of the core-electron excitations is responsible for the progressive enhancement of the plasmon peak with respect to the flat interband spectrum.

For both free and embedded clusters the displayed absorption spectra show that the quantitative agreement between the classical and hybrid models becomes more and more better as the size increases, as expected.

In Figures 7 and 8 are compared the predictions for free and embedded clusters, within models involving

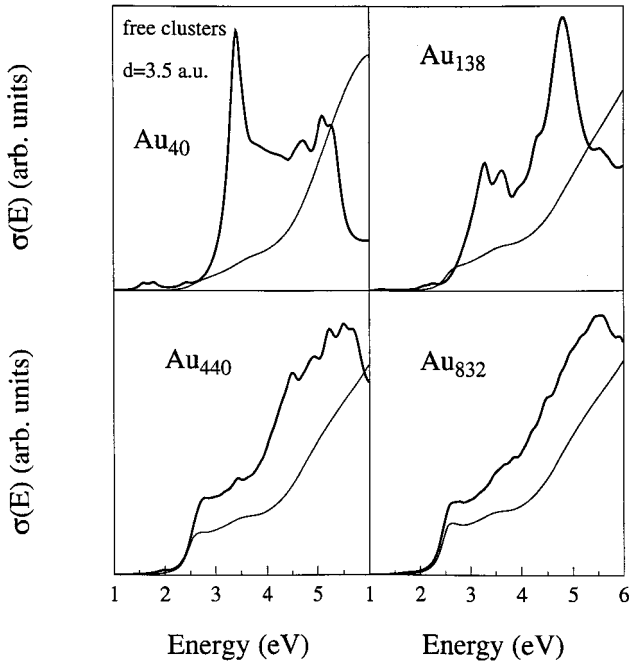

Fig. 7. Comparison between the results of the quantum model (thick line curves) and the classical Mie-theory (thin line curves), for free gold clusters involving an inner surface skin of ineffective screening (thickness $d = 3.5$ a.u.).

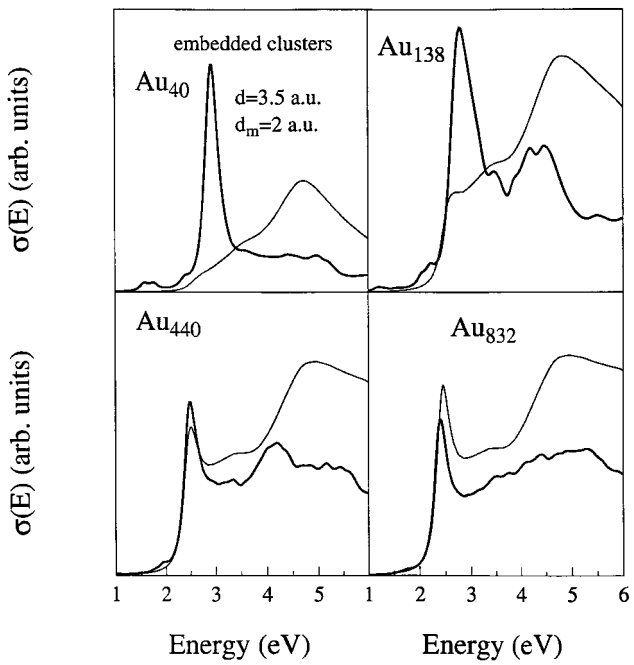

Fig. 8. Comparison between the results of the quantum model (thick line curves) and the classical Mie-theory (thin line curves), for alumina matrix-embedded gold clusters, within a model involving both an inner surface skin of ineffective polarizability (thickness $d = 3.5$ a.u.) and an outer vacuum rind simulating the local matrix porosity (thickness $d_m = 2$ a.u.).

surface skins of ineffective screening. Let us emphasize that, in these specific cases, the classical model involves two and three dielectric interfaces for free and embedded clusters, respectively, while the present mixed classical/quantum model involves one (free clusters) and two (embedded clusters) interfaces. In the classical theory (full dielectric description of each material) the ground-state step-walled electronic density fits perfectly the jellium distribution. Therefore the inner surface skin of ineffective screening (thickness d) is characterized by the Drude function $\varepsilon_2' = \varepsilon_s$, whereas the relevant dielectric function in the quantum model is the vacuum one $\varepsilon_2 = 1$. Hence, in the present approach, the cluster radius R_N is involved only for the ground-state calculations, and is no longer a dielectric interface in the optical response calculations.

Contrary to the previous simple models we can see that the discrepancies between the classical and present formalisms are now quantitatively *and* qualitatively very large for small cluster sizes. For free clusters the classical spectra do not even exhibit any structures over the entire spectral range, whereas sharp peaks are observed in the spectra calculated within the present model. For large clusters the surface plasmon band emerges only very weakly from the interband transitions, in both models, as in experiment [20] (second reference). These structures might be thought to reflect some "interference" between the interface modes. However, since the Fermi wavelength λ_F is much larger than the skin thicknesses, it is hazardous to interpret the quantum results in terms of such physical ingredients, and, except the plasmon peak, the structures are more probably specific small-size effects.

For the larger sizes $N = 440$ and $N = 832$ the qualitative agreement between both spectra is indeed unexpected, seeing that length scales much smaller than λ_F are involved in the physical system, namely d and d_m, and the induced electron densities are basically very different in both models. Since all the materials are homogeneous and no free charge density is present in the classical model, one has $\boldsymbol{\nabla} \cdot \mathbf{P}(\mathbf{r}) = 0$. Therefore all the induced polarization charge densities, related to, either the conduction, or the core electrons, are located at the interfaces $r = R_N - d$, R_N and $R_N + d_m$. In the present approach the induced electronic density $\delta n(\mathbf{r})$ is strongly inhomogeneous over the entire radial range $[0, R_N + d_m]$, and consequently the electric field $\mathbf{E}(\mathbf{r})$ inside the inner metal core $[0 < r < R_N - d]$ too, contrary to the pure classical case. In Figure 9 are displayed the real and imaginary components of the induced electron density in the cluster Au_{832}, for the photon energies $E = 2.4$ eV and $E = 4$ eV (thick line curves). Despite the large basic differences on the microscopic scale, both models yield rather similar qualitative results because the absorption cross-section is a global property, and only the total induced polarization charge density is relevant. In the hybrid model the conduction electrons give rise to the volume induced charge density $-\delta n(\mathbf{r}) = -\delta n(r)\cos(\theta)E_0$, and the core electrons to both,

(i) volume induced charge densities $-\boldsymbol{\nabla} \cdot \mathbf{P}_i(\mathbf{r})$ ($\mathbf{P}_i(\mathbf{r}) = [(\varepsilon_i - 1)/4\pi]\mathbf{E}(\mathbf{r})$ with $i = 1$ ($r < R_1$) and $i = m$ ($r > R_2$)), and,

(ii) interface induced charge densities at $R_1 = R_N - d$ and $R_2 = R_N + d_m$.

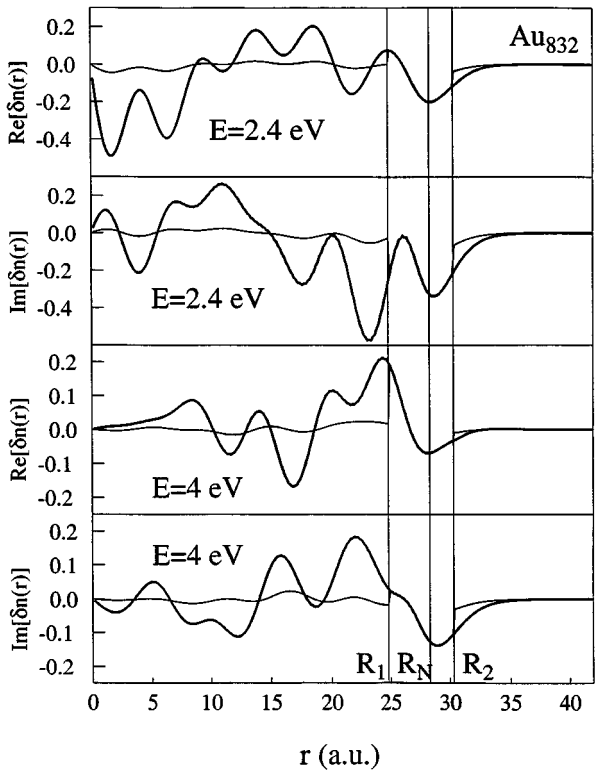

Fig. 9. The real and imaginary components of the induced conduction electron density in the cluster Au_{832}, for the excitation energies $E = 2.4$ eV and $E = 4$ eV (thick line curves). Thin line curves : minus the total volumic induced *charge* density, the induced polarization charges of the dielectric media included (see Sect. 3.2).

Owing to the homogeneity of the dielectric media and the Poisson equation $\Delta\phi(\mathbf{r}) = 4\pi\delta n(\mathbf{r})/\varepsilon_i$, the total volume induced polarization charge density $\rho(\mathbf{r}) = \rho(r)\cos(\theta)E_0$ is related to $\delta n(\mathbf{r})$ according to: $\rho(r) = -\delta n(r)/\varepsilon_1(\omega)$ $(r < R_1)$, $\rho(r) = -\delta n(r)$ $(R_1 < r < R_2)$ and $\rho(r) = -\delta n(r)/\varepsilon_m(\omega)$ $(r > R_2)$ (thin line curves in Fig. 9). Therefore, when media of high refractive indexes are involved, the induced conduction electron density is considerably quenched by the core electron polarization, except in the surface skins of ineffective screening. Obviously the interface induced densities differ in the two models, since the local electric field ($\mathbf{E}(\mathbf{r})$ at $r = R_1^-$ and $r = R_2^+$) and the dielectric functions (ε_i or ε_i') differ. This feature explains, *partly*, why both theoretical approaches lead to rather similar absorption spectra, and, moreover, why the classical Mie's theory works better for noble metal clusters, as compared to alkali species.

4 Summary and conclusions

In this paper a mixed quantum/classical model for calculating the light-absorption cross-section of a spherical multilayered metallic particle has been reported. The present theory can be applied to free or matrix-embedded particles with any number of concentric layers. In the model the conduction electron gas is quantum-mechanically treated in the framework of the Kohn-Sham DFT for the ground-state and the TDLDA theory for the optical response, while the optical properties of the various non-metallic media and of the metal ionic backgrounds are described through phenomenological dielectric functions. The present formalism improves considerably all the previous attempts to include, within the standard TDLDA formalism, dielectric effects from the ionic background and/or the surrounding matrix. Assuming the dipolar approximation, the optical response is calculated without additional physical or numerical approximations. All the screening and absorption properties of the various media, as well as their mutual influence, are self-consistently taken into account. The model has been exemplified in the case of free and matrix-embedded noble metal clusters. The results have been compared with those obtained by using the former models and with the predictions of the classical Mie-like theory. This analysis has clearly pointed out the deficiencies of the previous attempts, especially with regard to the definition of the *effective external field* in the TDLDA formalism and the global nature of the dynamical *matrix-embedded particle polarizability*. Moreover, it was emphasized that the light absorption by the various media is not directly related, as previously assumed, to the imaginary component of the total dipole corresponding to each medium. The slow convergence, over the whole spectral range, of the results obtained within the present approach towards the classical predictions has been illustrated. With regard to the previous works, we have checked that the finite-size-effect investigations on noble metal clusters, that were recently published by several authors, remain fortunately suitable, as long as only the size-dependence of the surface plasmon frequency is concerned.

Concerning the plasmon peak amplitude and broadening, its quenching by the interband transitions, and the absorption in the spectral range dominated by the core electron excitations, the present microscopical model is the only available one allowing a direct comparison with the experimental data, over the entire spectral range. Obviously the present formalism is only a first step towards a complete quantum description of the optical response of free or embedded small particles. For instance, refinements of the model could be attempted in order to improve the phenomenological description of the dielectric properties of the backgrounds. For instance dipole lattices with site-dependent polarizabilities could be substituted for the continuous media [7]. However, such a refinement, which requires to select a specific discrete geometry, would result in much more lengthy computations, contrary to the present approach. In particular, the spherical symmetry is broken, and the usual procedure consisting in spherically-averaging the conduction electron-background interaction for solving the ground-state problem (Kohn-Sham equations) does not seem consistent with the involved refinement. Nevertheless complete three-dimensional calculations on small particles would be interesting for testing to what extent the quenching of the induced electron density by the polarizable media is ensured in a discrete

environment. We think that, although the local screening and quenching effects would depend strongly on the position, the net effect, averaged over a length scale of a few nearest-neighbour atomic distances, would be similar to the one obtained in using continuous media.

The second point, about which model improvement should be gained in the future, concerns the bulk-like description of the dielectric properties of the ionic cores, which are assumed therefore *size-independent* (these approximations are assumed in the present work, as in previous approaches). As stated in the Introduction, refinement taking into account, in a self-consistent way (full quantum calculations or phenomenological size-dependent dielectric functions), the size effects affecting the interband transitions would be advised in further developments. Nevertheless experimental results on noble metal cluster anions and embedded clusters show that the size effects on the properties involving the *d*-band are much less pronounced as compared to those affecting the valence electrons [20]. For instance, the optical properties in the UV interband region, for both $Ag_N : Al_2O_3$ and $Au_N : Al_2O_3$ composite films, are quite well reproduced by the classical theory (Mie or Maxwell Garnett) involving the bulk dielectric functions. Strong discrepancies occur only around the plasmon band, and below the interband threshold. This strongly suggest that the use of a size-independent dielectric function for the ionic-core background is a rather good approximation.

Appendix A: Analytical expression for the dynamical polarizability $\alpha_{\delta n}$

In this appendix we prove the general formula equation (7). Equation (6) is multiplied by $r^2 f_c(r)$ and the integration is performed over the radial range $[a, b]$ (a and b are located in the same homogeneous layer i). Integrating $\int r^2 f_c(r)[\mathrm{d}^2 f_{\delta n}(r)/\mathrm{d}r^2]\mathrm{d}r$ by parts, one obtains (the r-dependence of the functions $f_c(r)$, $f_{\delta n}(r)$ and $\delta n(r)$ is omitted)

$$\left[r^2 f_c \frac{\mathrm{d}f_{\delta n}}{\mathrm{d}r}\right]_a^b - \int_a^b r^2 \frac{\mathrm{d}f_c}{\mathrm{d}r}\frac{\mathrm{d}f_{\delta n}}{\mathrm{d}r}\mathrm{d}r - 2\int_a^b f_c f_{\delta n}\mathrm{d}r = \frac{4\pi}{\varepsilon_i}\int_a^b r^2 f_c \delta n \mathrm{d}r. \quad (A.1)$$

The first integral (second term) is integrated by parts. Taking into account the fact that $f_c(r)$ obeys the Poisson equation (Eq. (6)) with $\delta n(r) = 0$, one obtains (after multiplication by ε_i)

$$\left[r^2\left(f_c\varepsilon_i\frac{\mathrm{d}f_{\delta n}}{\mathrm{d}r} - f_{\delta n}\varepsilon_i\frac{\mathrm{d}f_c}{\mathrm{d}r}\right)\right]_a^b = 4\pi\int_a^b r^2 f_c\delta n\mathrm{d}r. \quad (A.2)$$

The equation (A.2) is applied $(k+1)$ times to the following intervals:

$$(a,b) = [0, R_1[\,,]R_1, R_2[\,, \ldots,]R_{k-1}, R_k[\,,]R_k, \infty[\,.$$

The $(k+1)$ equations are then added. Using the boundary conditions at the interfaces $R_1, R_2, \ldots, R_k$, one obtains

$$\left[r^2\left(f_c\varepsilon_i\frac{\mathrm{d}f_{\delta n}}{\mathrm{d}r} - f_{\delta n}\varepsilon_i\frac{\mathrm{d}f_c}{\mathrm{d}r}\right)\right]_0^\infty = 4\pi\int_0^\infty r^2 f_c\delta n\mathrm{d}r. \quad (A.3)$$

Using the respective expressions of both potentials at large distance, namely $f_c(r) = (-r + b_m/r^2)$ and $f_{\delta n(}r) = \alpha_{\delta n}/(\varepsilon_m r^2)$, equation (A.3) reduces to

$$3\alpha_{\delta n} = 4\pi\int_0^\infty r^2 f_c\delta n(r)\mathrm{d}r. \quad (A.4)$$

Appendix B: model involving a single interface (radius R_1)

In this appendix explicit formula for a simple matrix-embedded metal sphere are given. The classical ingredients are listed below. The coefficients a_i and b_i (see Eq. (1)) are

$$a_1 = -\frac{3\varepsilon_m}{\varepsilon_1' + 2\varepsilon_m}, \quad b_m = \frac{\varepsilon_1' - \varepsilon_m}{\varepsilon_1' + 2\varepsilon_m}R_1^3. \quad (B.1)$$

The polarizability of the *matrix-embedded particle* (Eq. (2)) is thus

$$\alpha_c'(\omega) = \varepsilon_m\frac{\varepsilon_1' - \varepsilon_m}{\varepsilon_1' + 2\varepsilon_m}R_1^3. \quad (B.2)$$

For the quantum model, the ingredients involved in $f_c(r)$ (first term of the total electrostatic potential) are the same, namely a_1, b_m and $\alpha_c'(\omega)$ (notation $\alpha_c(\omega)$ in Sect. 2.2), except for the replacement of $\varepsilon_1'(\omega)$ by $\varepsilon_1(\omega)$ in the above expressions, where $\varepsilon_1(\omega)$ is the interband contribution to the metal dielectric function.

The polarizability $\alpha_{\delta n}(\omega)$ associated to the induced electronic density $\delta n(\mathbf{r})$, the directly-induced polarization charges included, is given by the equivalent following analytical expressions (Eq. (7))

$$\alpha_{\delta n}(\omega) = \frac{4\pi}{3}\left[a_1\int_0^{R_1} r^3\delta n(r)\mathrm{d}r + \int_{R_1}^\infty \left[b_m - r^3\right]\delta n(r)\mathrm{d}r\right], \quad (B.3)$$

$$\alpha_{\delta n}(\omega) = \frac{4\pi}{3}\left[a_1\int_0^\infty r^3\delta n(r)\mathrm{d}r + \frac{b_m}{R_1^3}\int_{R_1}^\infty \left(R_1^3 - r^3\right)\delta n(r)\mathrm{d}r\right]. \quad (B.4)$$

References

1. U. Kreibig, M. Vollmer, *Optical Properties of Metal Clusters* (Springer, Berlin 1995) and references therein.
2. G. Mie, Ann. Phys. (Leipzig) **25**, 377 (1908).
3. W.A. de Heer, Rev. Mod. Phys. **65**, 611 (1993) and references therein.
4. M. Brack, Rev. Mod. Phys. **65**, 677 (1993) and references therein.
5. Ll. Serra, A. Rubio, Z. Phys. D **40**, 262 (1997).
6. J. Lermé, B. Palpant, B. Prével, M. Pellarin, M. Treilleux, J.L. Vialle, A. Perez, M. Broyer, Phys. Rev. Lett. **80**, 5105 (1998).
7. Ll. Serra, A. Rubio, Phys. Rev. Lett. **78**, 1428 (1997).
8. J. Lermé, B. Palpant, B. Prével, E. Cottancin, M. Pellarin, M. Treilleux, J.L. Vialle, A. Perez, M. Broyer, Eur. Phys. J. D **4**, 95 (1998).
9. C. Yannouleas, R.A. Broglia, M. Brack, P.F. Bortignon, Phys. Rev. Lett. **63**, 255 (1989).
10. M.J. Stott, E. Zaremba, Phys. Rev. A **21**, 12 (1980).
11. A. Zangwill, P. Soven, Phys. Rev. A **21**, 1561 (1980).
12. W. Ekardt, Phys. Rev. B **31**, 6360 (1985).
13. V. Bonacic-Koutecky, P. Fantucci, J. Koutecky, Chem. Rev. **91**, 1035 (1991).
14. M.J. Puska, R.M. Nieminen, M. Manninen, Phys. Rev. B **31**, 3486 (1985).
15. A. Rubio, Ll. Serra, Phys. Rev. B **48**, 18222 (1993).
16. L.I. Kurkina, O.V. Farberovich, Phys. Rev. B **54**, 14791 (1996).
17. V.V. Kresin, Phys. Rev. B **51**, 1844 (1995).
18. A.A. Lushnikov, A.J. Simonov, Z. Phys. **270**, 17 (1974).
19. J. Sinzig, U. Radtke, M. Quinten, U. Kreibig, Z. Phys. D **26**, 242 (1993).
20. This hypothesis seems to be supported by ultraviolet photoelectron experiments on small noble metal clusters (K.J. Taylor *et al.*, J. Chem. Phys. **96**, 3319 (1992)) and ellipsometry measurements on Au_N/Al_2O_3 films involving various size distributions (B. Palpant *et al.*, Phys. Rev. B **57**, 1963 (1998)).
21. $\mathbf{E} = -\boldsymbol{\nabla} V - \partial \mathbf{A}/\partial t$ where $\mathbf{A}$ is the potential vector. In the dipolar approximation the ratio between the two terms is on the order of $(\lambda/R)^2$.
22. C. Yannouleas, R.A. Broglia, Ann. Phys. (NY) **217**, 105 (1992).
23. A. Liebsch, Phys. Rev. Lett. **71**, 145 (1993).